Transmission of entangled photons studied by quantum tomography

Remy, Mathilde; Bokic, Bojana; Cormann, Mirko; Kubo, Wakana; Caudano, Yves; Kolaric, Branko

Published in:
Journal of Physics Communications

DOI:
10.1088/2399-6528/ab292f

Publication date:
2019

Document Version
Publisher's PDF, also known as Version of record

Transmission of entangled photons studied by quantum tomography: do we need plasmonic resonances?

Journal of Physics Communications

PAPER

Transmission of entangled photons studied by quantum tomography: do we need plasmonic resonances?

Mathilde Remy[1], **Bojana Bokic**[2], **Mirko Cormann**[1], **Wakana Kubo**[3], **Yves Caudano**[1,5] and **Branko Kolaric**[2,4,5]

[1] Department of Physics, University of Namur, Rue de Bruxelles 61, 5000 Namur, Belgium
[2] Institute of Physics, University of Belgrade, Pregrevica 118, 11080 Belgrade, Serbia
[3] Department of Electrical and Electronic Engineering, Tokyo University of Agriculture and Technology, 2-24-16 Naka-cho, Koganei-shi, Tokyo 184-8588, Japan
[4] Micro- and Nanophotonic Materials Group, University of Mons, Place du Parc 20, 7000 Mons, Belgium
[5] Authors to whom any correspondence should be addressed.

E-mail: yves.caudano@unamur.be **and** branko.kolaric@umons.ac.be

Keywords: quantum entanglement, quantum tomography, plasmonic, nanoscale optics

OPEN ACCESS

RECEIVED
23 April 2019

REVISED
24 May 2019

ACCEPTED FOR PUBLICATION
12 June 2019

PUBLISHED
26 June 2019

Abstract

We performed quantum tomography to reveal the robustness of quantum correlations of photons entangled in polarisation after their interaction with plasmonic and nonplasmonic environments at normal incidence. The experimental findings clearly show that the visibility of quantum correlations survives the interaction, and that the presence of plasmonic resonances has not any significant influence on the survival of polarisation correlations for transmitted photon pairs. The results indicate that quantum states can be encoded into the multiple motions of a many-body electronic system without demolishing their quantum nature. The plasmonic structures and their resonances only enhance the overall transmission. Thus, they could benefit the pair detection rate, that is the number of coincidences per unit of time, but they do not affect the visibility of quantum correlations. We also performed quantum tomography of the entangled pairs after interaction with the continuous planar gold film as a function of the incidence angle. The latter illustrates the loss of polarization correlations that arises from the partially polarizing properties of the isotropic sample out of normal incidence. Our work shows that plasmonic structures are not needed to exploit quantum entanglement if the rate of coincidence counting is sufficient.

1. Introduction

Recently a few articles [1–3] described and thoroughly discussed the importance of polaritonic structures and plasmonic resonances for the survival of quantum entanglement in polarization or energy (frequency bin entanglement). Surface plasmon polaritons (SPPs) are quasi-particles created by the coupling of light with collective oscillations of the conduction electrons at a metal-dielectric interface. SPPs exhibit an evanescent field in the direction perpendicular to their propagation. Therefore, they strongly confine light at the interface. Metallic nanostructures can convert photons into SPPs, which tunnel through the structure before reradiating as photons [4, 538]. This photon-plasmon-photon conversion process has been investigated with polarisation [1, 39] (see also the theoretical analysis of [6]), time-bin [2, 7] and orbital-angular-momentum [8] entanglement. It has been shown that plasmons maintain nonclassical photon statistics, and preserve entanglement, encoding entangled photons in multi-electronic systems.

The work of Olislager *et al.* [2] reviewed different quantum experiments with plasmons, such as Young's double-slit experiment [9], evidence of quantum superpositions of single plasmons [10–14], and the generation of plasmonic squeezed states [15], as well as two-particle experiments [16–21]. The studies mentioned above proved the quantum bosonic nature of plasmonic excitations. It has also been shown that the spin–orbit coupling of incident light allows the post-selection of the final state in a quantum weak measurement of the light

chirality [22]. The polarisation entanglement of photon pairs [1], as well as energy-time entanglement, are preserved [2] in cascading photon to SPP and subsequently to photon conversions, with preservation of temporal coherence that is larger than the SPP lifetime [7]. Besides, both the quasi-particle and wave nature of SPP are highlighted in experiments similar to those attesting the wave-particle duality of photons when they interact with beam splitters [12].

For these reasons, the advantages of quantum plasmonics have gained much visibility in the physical community [1–3, 23], since plasmons and SPPs or localized surface plasmon resonances (LPSRs) offer the unique possibility to control and manipulate nonclassical states of light. Integrated quantum technologies that allow scalability and miniaturization, as well as coherent coupling to single emitters [3, 4, 24] harnessing plasmonic resonances, offer a great potential for multiple applications in quantum information and technology, such as design and fabrication of single-photon sources, transistors, and ultra-compact circuitry, with potential applications for secure communication and advanced computing [25–27].

Here, we go further into the characterization of the entanglement preservation properties of thin metallic structures. We study not only the visibility of the coincidence detections but the full quantum state and correlations after transmission, i.e. after interaction with corrugated and noncorrugated metallic films. In this particular study, we use photons entangled in polarisation at a near-infrared wavelength (818 nm) and investigate the interaction of the photons with an entirely different metallic structure, a continuous planar gold film, in order to reveal by quantum tomography the robustness of quantum correlations in the absence of plasmonic resonance.

2. Experimental part

A planar and continuous metallic film with thickness of 10 nm (3 nm Cr + and 7 nm Au) was deposited by thermal sputtering on a glass substrate. The precise thicknesses of the deposited Cr and Au layers were determined using the Rutherford Back Scattering method (RBS) after deposition.

The anisotropic, chiral plasmonic structures were fabricated by electron beam lithography [28] and lift-off process. They were drawn on a resist thin film (Zeon Corporation, ZEP-520a) on a transparent substrate. Chromium and gold films of 5 and 20 nm (total thickness of 25 nm) were deposited on the patterned resist film by thermal deposition technique. After the lift-off process, the anisotropic, chiral plasmonic arrays were obtained. The geometry of the array and a high resolution image of the plasmonic units are presented in figure 1.

3. Quantum optical setup

Initially, a half-wave plate and a polarising beam splitter prepare the polarisation of the pump laser beam at 45° with a central wavelength at 409 nm (see figure 2). Photon pairs with a double central wavelength are produced via spontaneous parametric downconversion within two orthogonal and superimposed BBO-crystals of type I [29]. Nonlinear crystals are oriented such that horizontal and vertical polarisations participate in the downconversion within the first and the second crystal, respectively. A third BBO-crystal is placed in front of the source to compensate the group velocity mismatch. This configuration allows us to prepare a maximally entangled Bell State $|\phi_+\rangle = \frac{1}{\sqrt{2}}(|HH\rangle + |VV\rangle)$.

In the second part of the setup, a half-wave plate, a quarter-wave plate and a polarising beam splitter are placed along each optical path of photon pairs. Photons are detected with four single-photon-counting modules (SPCM) and a field-programmable gate array (FPGA) coincidence counter. Count and coincidence counting are used to make polarisation measurements. This means that single-photon detection event resulting from losses along one optical path (due for example to reflection, absorption, or scattering) are not considered for quantum tomography, as only photon correlations are taken into account. (Technically: we only probe the two-photon subspace of the Hilbert space.) Different basis are adjusted with the combined orientations of wave plates. Iris and low-pass filters select the desired superposed emission cones and reduce noise. Complementary information on the optical and detection setup can be found in [30].

4. Results and discussion

4.1. Transmission spectrum of the planar and nanostructured metallic film

The transmission (T) spectra of the gold films were measured at normal incidence with the UV–Vis Cary spectroscope on circular areas of 0.5 cm diameter. The spectrum of the noncorrugated gold film (see figure 3, upper) exhibits the well-known spectrum of a semi-transparent film, as it is rather opaque in the visible range [31]. The optical spectrum of the plasmonic nanostructures is also presented (see figure 3, lower). The optical

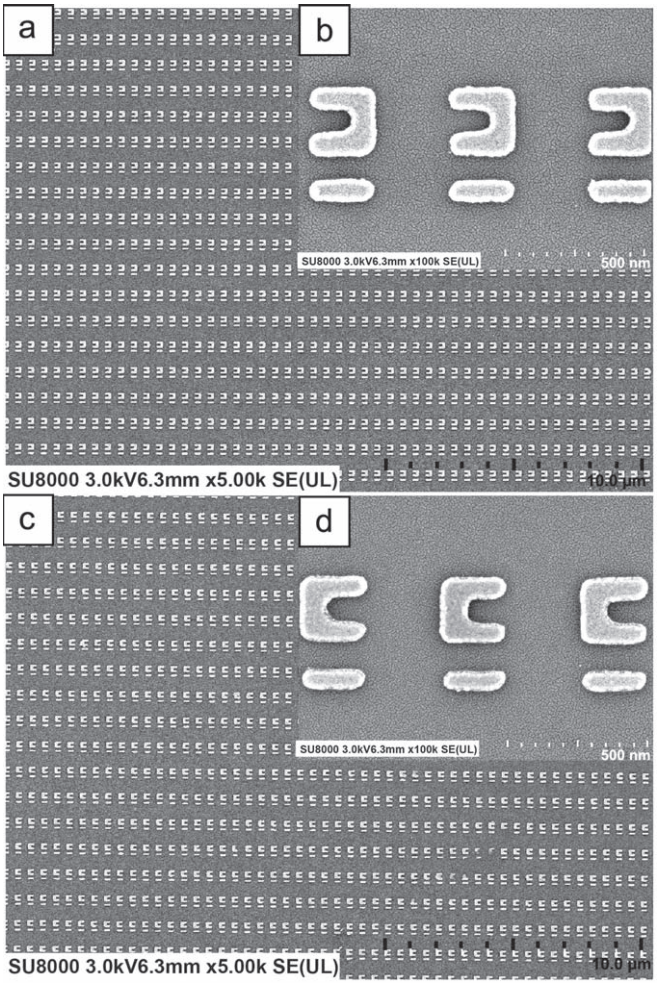

Figure 1. SEM image of the anisotropic chiral plasmonic nanostructures (upper-a: left handed; lower-c: right handed). The insets are large magnification images of the left-handed (upper-b) and right-handed (lower-d) chiral plasmonic structures. The scale bars in the insets are 500 nm. The distance between the structures as well as the height and the broadest width of the C-like structures are approximately 250 nm. The length of the rods is also approximately 250 nm while the corresponding width is about 84 nm. The different structures were deposited on the same substrate near each other using lithography method (see Experimental Part).

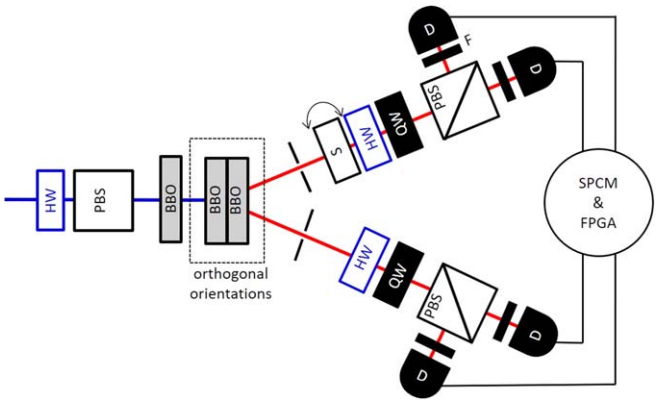

Figure 2. Experimental setup. Red lines represent the optical path of frequency-degenerate photon pairs. HW (half-wave plate), PBS (polarising beam splitter), BBO (BBO-crystal of type I), QW (quarter-wave plate), F (low-pass filter), D (lens and fibre coupler to SPCM) and sample (S). The sample is put in one of the two, otherwise equivalent, optical paths. It can rotate around an axis perpendicular to the optical table to change the angle of incidence.

properties of metallic particles are influenced by the particle size and orientation. The optical spectrum of plasmonic nanostructures is significantly structured. Due to the anisotropy and chirality of the array, a small difference in transmission (on different parts of the array) can be observed using different polarizations of the

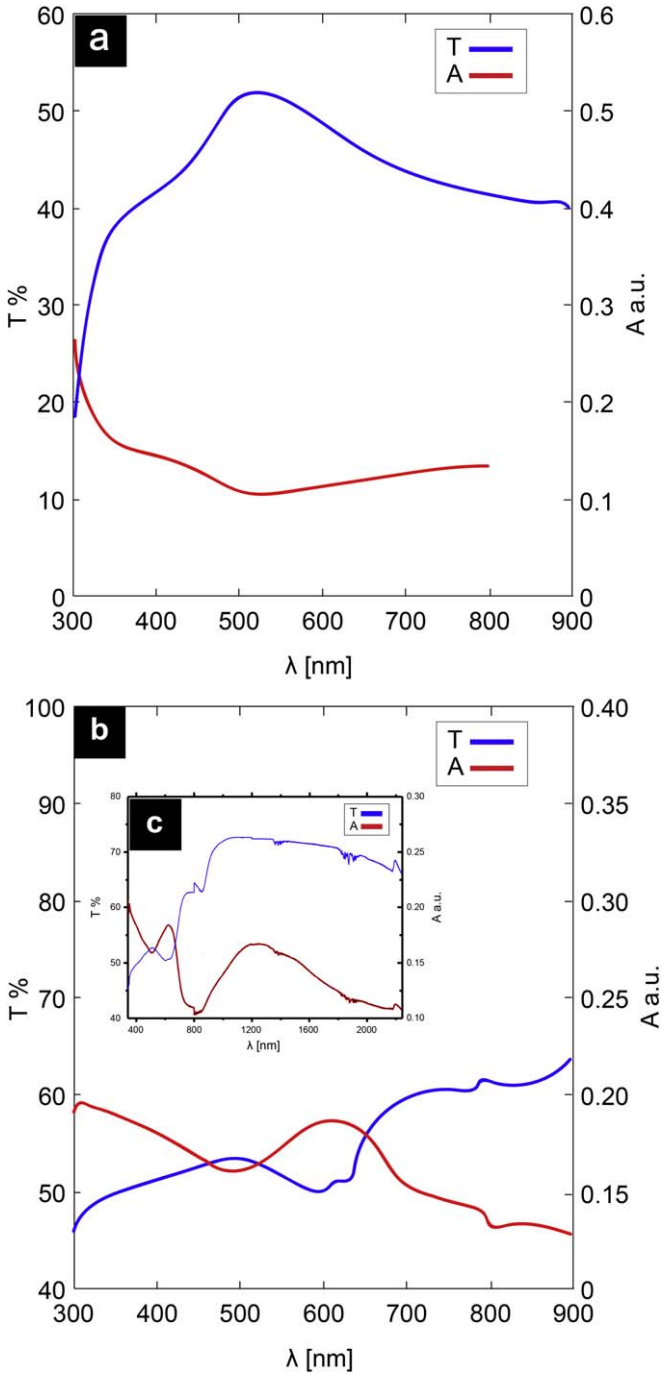

Figure 3. Optical Spectra of planar (upper-a) and nanostructured (lower-b) metallic films. Transmission curves are in blue while absorbance curves are in red. The inset (c) shows the optical spectra of the nanostructured sample over a wavelength range exhibiting also near-IR plasmonic resonances.

incident light (results not shown). In our experimental results depicted in figure 3, transmission and absorption of both the continuous and structured metallic films were measured using nonpolarized light and through a large spot, so that it was not possible to observe the small difference in transmission related to the anisotropy and chirality of the array. Thanks to the plasmonic resonances, the overall transmission of the nanostructured film increases, and becomes larger than the continuous planar film (see figure 3), even though the nanostructured film is thicker than the continuous film (25 versus 10 nm). It exhibits resonances with an asymmetric peak, which resembles very much the one previously reported for extraordinary transmission of different metallic subwavelength nanostructures [2, 31, 32]. In the case of the structured film, the peak in the absorption probably arises from the excitation of dipolar mode of the plasmonic array.

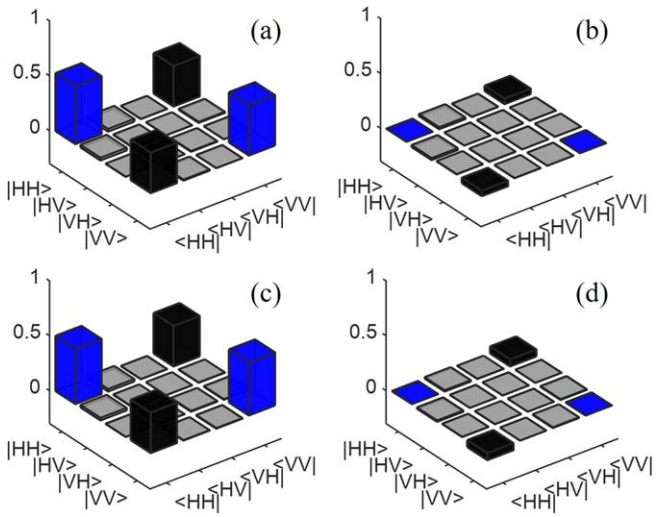

Figure 4. Graph of the real (left) and imaginary (right) parts of the density matrix. Graphs (a) and (b) represent the density matrix $\hat{\sigma}$ of the biphoton state after transmission through the structured plasmonic film. Graphs (c) and (d) represent the density matrix $\hat{\rho}$ of the initial biphoton state. Blue rods and black rods represent diagonal and off-diagonal terms of the density matrix, respectively.

4.2. Quantum tomography with the nanostructured metallic film at normal incidence

We start by evaluating the effect of the plasmonic nanostructures on polarisation-entanglement, in transmission. We realise a quantum tomography to reconstruct the density matrix of the system of the initial biphoton state $\hat{\rho}$ obtained without the sample and the state $\hat{\sigma}$ obtained after transmission through the sample with the plasmonic nanostructures and at normal incidence. We realise quantum tomography of a system of two qubits with two detectors per qubit. In this case, 9 different measurement bases are sufficient to realise the quantum tomography [33]. Although using 36 different analysis settings can improve the measurement precision, in order to minimise the total time of tomography and increase the stability during the complete course of measurements, quantum tomography is performed with 9 different bases. Each basis measurement without and with the nanostructured sample is realised within a time total of 60 s and with a time window of 16 ns for coincidence counting. All results are treated with the code developed by Paul Kwiat's quantum information group to determine the maximum likelihood estimation of each state, the metrics describing the features of the quantum state and its uncertainties [33, 34]. The fidelity $F(\hat{\rho}_1, \hat{\rho}_2) = (Tr[\sqrt{\sqrt{\hat{\rho}_1}\ \hat{\rho}_2\ \sqrt{\hat{\rho}_1}}\ ])^2$ is a measurement of similarity between the two states $\hat{\rho}_1$ and $\hat{\rho}_2$ and can take value in the interval [0,1]. In our experiment, $F(\hat{\rho}, \hat{\sigma}) = 0.9966 \pm 0.0012$ is very close to one. Furthermore the computed fidelities with the Bell state $|\phi_+\rangle$, $F(|\phi_+\rangle, \hat{\rho}) = 0.8630 \pm 0.0018$ and $F(|\phi_+\rangle, \hat{\sigma}) = 0.8627 \pm 0.0012$ are nearly identical. These show that the initial and final states are nearly identical. We conclude that, at normal incidence, the nanostructured sample does not change significantly the polarisation, the polarisation correlations, and the entanglement of the transmitted photon pairs. This is confirmed by the similarity between the graphical representations of these states (see figure 4). These results are in line with previous observations, which indicate that plasmonic nanostructures are able to preserve entanglement [1, 2].

4.3. Quantum tomography with the continuous metallic film at normal incidence and as a function of the incidence angle

In order to assess the effect of plasmonic resonances on preserving quantum correlations, we performed a detailed quantum tomography study on the planar structure without plasmonic resonances. For classical waves, our continuous, planar film does not affect the polarisation at normal incidence. Transmittance is the same for all polarisations as it is isotropic in the surface plane. For non-normal incidence, the transmittance becomes a function of the polarisation. We investigate the effect of introducing the sample with different angles of incidence on the entangled polarisation state produced by the quantum source, as described below.

Firstly we measure both the initial biphoton state $\hat{\rho}$ obtained without the sample and the state $\hat{\sigma}$ obtained after transmission through the continuous metallic film at normal incidence. We realise a quantum tomography to reconstruct the density matrix of the system. Polarisation measurements are made in 36 different bases. Each measurement without (with) the planar sample is realised within a time total of 30 s (60 s) and with a time window of 16 ns (16 ns) for coincidence counting. The graphical representations of these states are also very similar (see figure 5).

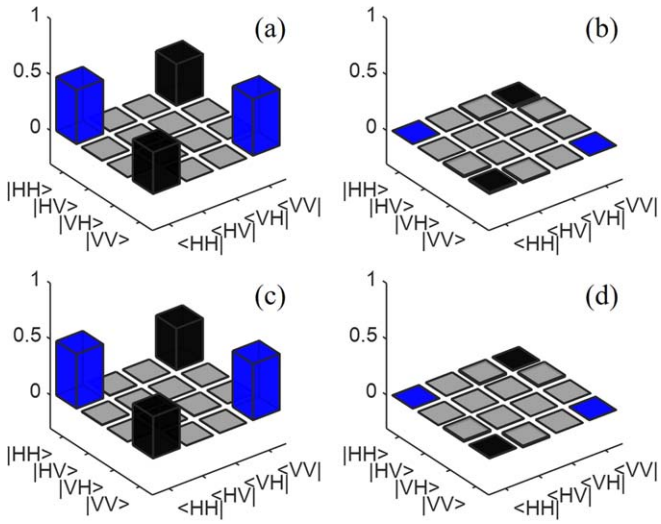

Figure 5. Graphical representation of the density matrix estimated by quantum tomography. The value of the real (a) and imaginary (b) parts of the density matrix $\hat{\sigma}$ of the biphoton state after transmission through the continuous metallic film and the value of the real (c) and imaginary (d) parts of the density matrix $\hat{\rho}$ of the initial biphoton state. Blue rods and black rods represent diagonal and off-diagonal terms of the density matrix, respectively.

The fidelity between the two states $F(\hat{\rho}, \hat{\sigma}) = 0.9989 \pm 0.0003$ is very close to one. In other words, the two-photon states before and after the sample at normal incidence are closely similar. Furthermore, the computed fidelities with the Bell state $|\phi_+\rangle$, $F(|\phi_+\rangle, \hat{\rho}) = 0.8683 \pm 0.0008$ and $F(|\phi_+\rangle, \hat{\sigma}) = 0.8673 \pm 0.0006$ are nearly identical and lead to the same conclusion. At normal incidence the thin, continuous, metallic film does not change significantly the polarisation of the transmitted photon pairs. Consequently, polarisation entanglement is completely preserved within the experimental uncertainties.

Secondly, we compare the initial, unperturbed state $\hat{\rho}_0$ and the states obtained after the sample with 4 different orientations: at normal incidence ($\hat{\sigma}_0$), 20° ($\hat{\sigma}_1$), 35° ($\hat{\sigma}_2$) and 50° ($\hat{\sigma}_3$) with respect to the surface normal. In order to maximise the stability of the experiment throughout the measurements, quantum tomography is performed with 9 different bases with a total time of 60 s for each basis measurement and a coincidence time window of 16 ns. To compare the measured quantum state to the expected state produced by each sample rotation (0°, 20°, 35° and 50°), we calculate the theoretical renormalized state of the system after the sample:

$$\hat{\sigma}_t = \frac{(\hat{M}\hat{\rho}_0\hat{M}^\dagger)}{Tr\,(\hat{M}\hat{\rho}_0\hat{M}^\dagger)} \text{ with } \hat{M} = \hat{I} \otimes (t_H\hat{P}_H + t_V\,\hat{P}_V),$$

which we evaluate using the theoretical complex transmission coefficients through the metallic film sample of $p(t_H)$ and $s(t_V)$ polarisations and the projectors $\hat{P}_H$ and $\hat{P}_V$ on the horizontal and vertical polarisation states, respectively. As the transmission coefficients are complex numbers, the impact of phase differences between the transmitted *s* and *p* polarisations is taken into account in our evaluation of the transmitted two-photon state and in our calculations of the fidelities to the initial state. The transmission coefficients are obtained numerically with the matrix transfer method applied to flat multilayers of Au/Cr/glass, with thickness of 7 nm/3 nm/1 mm respectively. We use the complex refractive index at wavelength $\lambda = 818$ nm for the gold $n_{Au} = 0,15905 + 5,0572\,i$ [35], chromium $n_{Cr} = 3,1945 + 3,4772\,i$ [36] and glass N-BK7 (SHOTT) $n_{glass} = 1,5104 + 9,3260.10^{-9}\,i$ obtained from [37]. Rapid oscillations of small amplitude of the wavelength-dependent transmission coefficients were averaged out. These arise from multiple reflections between the optical interfaces. They are not observed experimentally due to the finite coherence time and beam size.

The entanglement of formation $E_f(\hat{\sigma})$ is a measurement of entanglement for a state $\hat{\sigma}$. For a system of two qubits, $E_f(\hat{\sigma}) = -x\log_2(x) - (1-x)\log_2(1-x)$ with $x = \frac{1+\sqrt{1-C^2}}{2}$ and the concurrence $C = \max(\lambda_4 - \lambda_3 - \lambda_2 - \lambda_1, 0)$ where λ_i with $i = 1,2,3,4$ are the square roots of the eigenvalues of $\hat{\rho}(\hat{\sigma}_y \otimes \hat{\sigma}_y)\,\hat{\rho}^*(\hat{\sigma}_y \otimes \hat{\sigma}_y)$ in increasing order. We measure the entanglement of formation $E_f(\hat{\sigma}_i)$ and the experimental state fidelity with respect to the state without the sample $F(\hat{\rho}_0, \hat{\sigma}_i)$, and with respect to the maximally entangled Bell state theoretically produced $F(|\phi_+\rangle, \hat{\sigma}_i)$. These properties quantify the influence of the planar film on the entanglement and polarisation state of the transmitted photon pairs. As our aim is to quantify the preservation of quantum entanglement in transmission through the sample, we first measure and compute the entanglement of

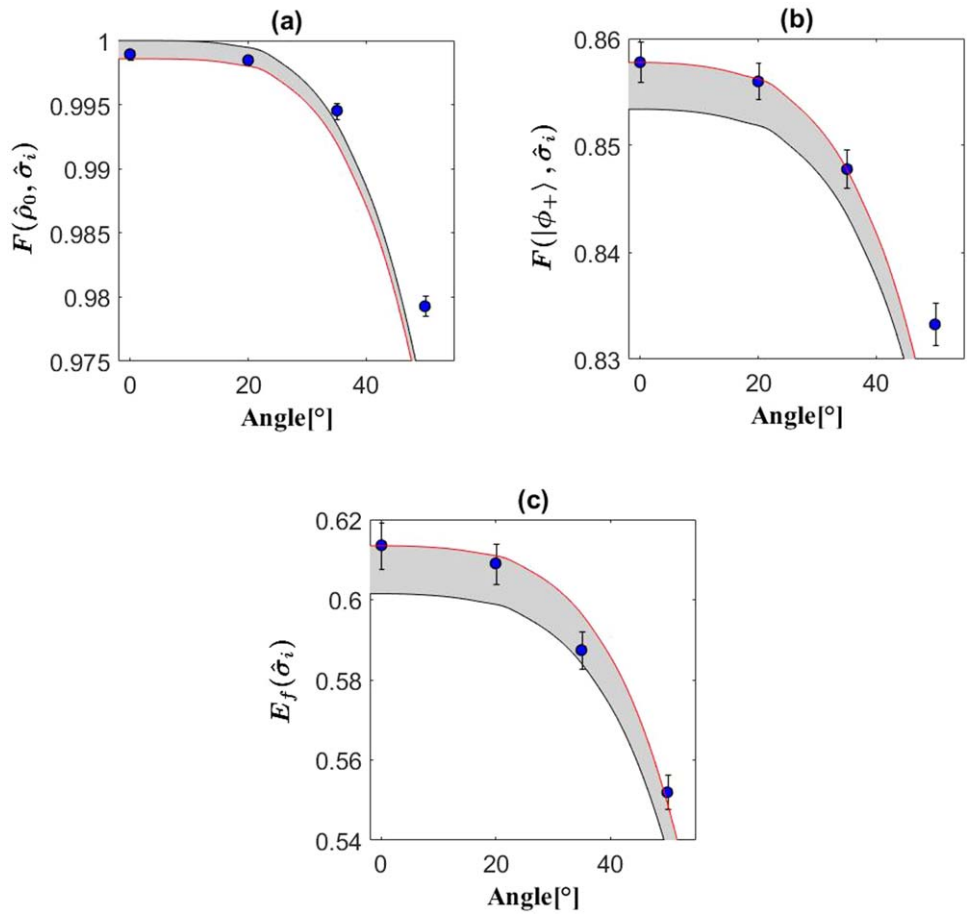

Figure 6. (a) Graph of the fidelity $F(\hat{\rho}_0, \hat{\sigma}_i)$ between the polarisation state with the continuous metallic film $\hat{\sigma}_i$ and without the sample $\hat{\rho}_0$ in function of the angle of incidence, i.e. of the rotation of the sample; (b) Graph of the fidelity $F(|\phi_+\rangle, \hat{\sigma}_i)$ with respect to the maximally entangled Bell state; (c) Graph of the measure of entanglement of formation $E_f(\hat{\sigma}_i)$ of the polarisation state with the sample $\hat{\sigma}_i$ in function of the angle of incidence. (a)–(c) Error bars represent the statistical error evaluated with a Monte Carlo method. Theoretical curves are calculated with the theoretical renormalized state $\hat{\sigma}_t$. For each graphic, there are two theoretical curves, calculated with respect to the two reference states $\hat{\rho}_0$ (in black) and $\hat{\sigma}_0$ (in red). We use two curves because theoretically the density matrix of the state with and without the sample at normal incidence should be the same, as confirmed experimentally (fidelity between them nearly equal to 1). The area between the two theoretical curves is filled in grey.

formation. However, the degree of entanglement can be left unchanged by transmission while the state is transformed to another (equally) entangled state. For this reason, it is also important to quantify the closeness between the states before and after transmission through the sample, which we do by calculating the fidelity. In theory, the state of the photon pairs transmitted through the planar sample at normal incidence $\hat{\sigma}_0$ should be the same as in the configuration without the sample $\hat{\rho}_0$. This is confirmed experimentally with the measure of the fidelity $F(\hat{\rho}_0, \hat{\sigma}_0)$, which is nearly equal to one. This is an immediate consequence of the equality between the transmission coefficients for *s* and *p* polarisations. For this reason, we use both $\hat{\rho}_0$ and $\hat{\sigma}_0$ as a reference to calculate the theoretical fidelity with respect to the initial state as a function of the incidence angle (see figure 6). We use these two references to provide a bound on experimental uncertainties due to the global stability of the system over long acquisition times. The theoretical curves associated with these two references are really close to each other, as shown by the *Y*-axis scales. The experimental entanglement of formation $E_f(\hat{\sigma}_i)$ and the fidelities $F(|\phi_+\rangle, \hat{\sigma}_i)$ and $F(\hat{\rho}_0, \hat{\sigma}_i)$ decrease slowly with the angle of incidence (see figure 6) and are in agreement with the theoretical predictions.

For each state $\hat{\sigma}_i$ with $i \in \{0, 1, 2, 3\}$, quantum tomography reveals that the probability of measuring a final polarisation $|HH\rangle$ ($|VV\rangle$) after the planar, continuous, metallic film increases (decreases) with the angle of rotation of the sample (see figure 7). The asymmetry between the coloured diagonal rods (blue or red) increases with the angle. This is explained by the fact that, out of normal incidence, the transmission coefficient of *p* polarisation is larger than the transmission coefficient of *s* polarisation. We quantify this behaviour experimentally and we compare it with theory (see figure 8). We represent the probabilities of measuring a final

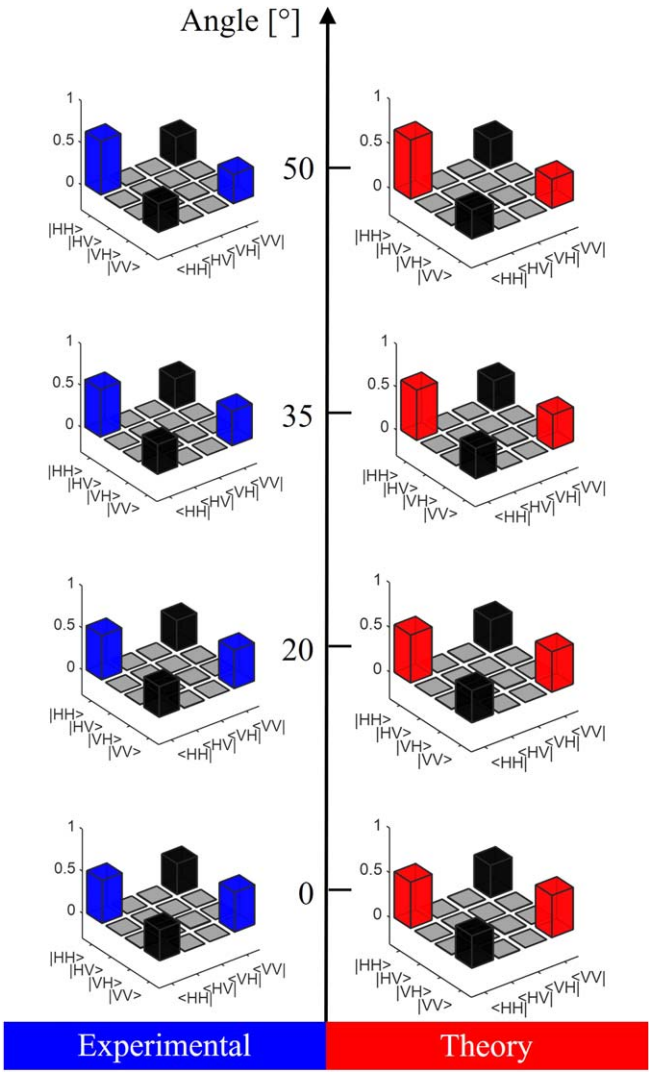

Figure 7. On the left (right), the graphical representation of the experimental (theoretical) values of the real parts of the density matrix $\tilde{\sigma}_i$ of the biphoton state after transmission through the continuous metallic film in function of the angle of incidence, i.e. of the rotation of the sample.

polarisation $|HH\rangle$ and $|VV\rangle$ of a system in an initially entangled state like the $|\phi_+\rangle$ Bell state. Each point represents the mean value of 30 measurements of 5 s.

We conclude that the introduction of the flat, metallic film sample at normal incidence decreases the coincidence rate (a loss of $\sim$55% theoretically and $\sim$57% experimentally) but it does not affect the entangled quantum state. Without perturbation of the polarisation of the system, the density matrix of the polarisation degree of freedom remains the same. This occurs at normal incidence, since the sample does not have any polarising property. For non-normal incidence, the polarisation entanglement decreases. It is related to the different transmission coefficients of *s* and *p* polarisation through the sample. This fact indicates that quantum correlations will be affected only if polarisation is affected. Although the nanostructured sample provides a transmission $\sim$50% better than the planar metallic film, the fidelities and trace distance between the initial and transmitted states at normal incidence indicate that the initial state preservation is nevertheless (marginally) better in the case of the planar metallic film. This effect could be the result of the anisotropy of the nanostructured sample that induces a small polarising effect upon transmission at normal incidence, contrary to the planar, isotropic film.

5. Conclusion

In the present work, we studied the preservation of polarisation entanglement in transmission through nanostructured and continuous planar gold films using quantum tomography. The quantum correlations survive after interaction with planar films and our finding clearly indicates that plasmonic resonances do not

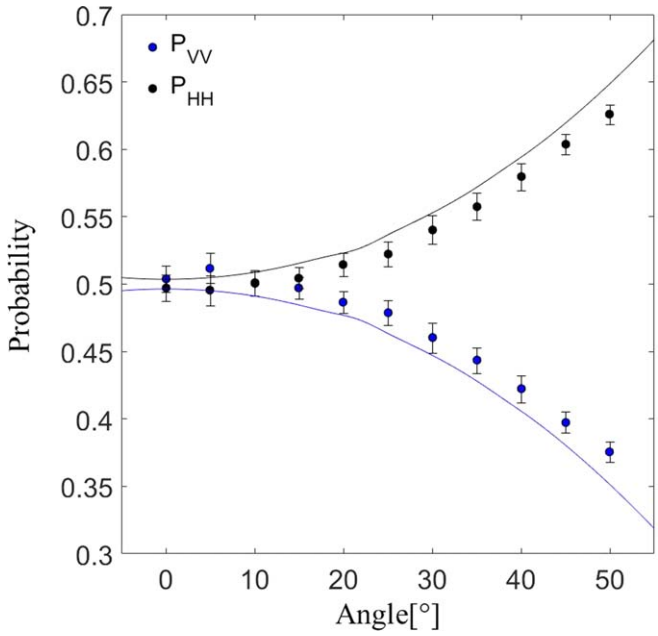

Figure 8. Probability of measuring a final polarisation $|HH\rangle$ (black) and $|VV\rangle$ (blue) after transmission through the continuous metallic film in function of the angle of incidence, i.e. of the rotation of the sample. Error bars represent the standard deviation of 30 measurements. Continuous curves represent the theoretical probabilities, P_{HH} and P_{VV}, as a function of the rotation of the sample.

play any significant role in the robustness of correlation preservation. They may only improve potentially the total coincidence rate by increasing the transmission coefficient through the film, while they do not play any role *per se* in the preservation of entanglement in the quantum state of the transmitted photon pairs.

Acknowledgments

All authors acknowledge Mr Adrien Nélis, Dr Sébastien Mouchet, Mr Bruno Majérus, and Dr Jean-François Colomer for their assistance in the characterization of the continuous metallic film. This work made use of the OLS, SIAM, and MORPH-IM technological platforms of the University of Namur, with support from the NISM and naXys Institutes. B K acknowledges financial support from the 'Action de Recherche Concertée' (BIOSTRUCT project, No. 10/15-033) of UNamur and from Interuniversity Attraction Pole: Photonics@be (P7-35, Belgian Science Policy Office). B K and B B acknowledge financial support of the Ministry of Science, Republic of Serbia (grant III 45016). B K and Y C acknowledge support from Nanoscale Quantum Optics COST-MP1403 action and from F R S-FNRS. Y C is a research associate of the Belgian Fund for Scientific Research F R S-FNRS.

ORCID iDs

Mathilde Remy https://orcid.org/0000-0002-4101-0454
Bojana Bokic https://orcid.org/0000-0002-9061-7201
Yves Caudano https://orcid.org/0000-0002-0805-4068
Branko Kolaric https://orcid.org/0000-0003-0203-7897

References

[1] Altewischer E, Van Exter M P and Woerdman J P 2002 *Nature* **418** 304–6
[2] Olislager L, Kubo W, Tanaka T, Ungureanu S, Vallée R, Kolaric B, Emplit P and Massar S 2015 *Nanophotonics* **4** 324–31
[3] Jacob Z 2012 Quantum plasmonics *Mrs Bull.* **37** 761–7
[4] Ebbesen T W, Lezec H J, Ghaemi H F, Thio T and Wolff P A 1998 *Nature* **391** 667–9
[5] Martín-Moreno L, García-Vidal F J, Lezec H J, Pellerin K M, Thio T, Pendry J B and Ebbesen T W 2001 *Phys. Rev. Lett.* **86** 1114
[38] Büse A, Juan M, Tischler N, D'Ambrosio V, Sciarrino F, Marrucci L and Molina-Terriza G 2018 *Phys. Rev. Lett.* **121** 173901
[39] Chen Y, Lee C, Lu L, Liu D, Wu Y, Feng L, Li M, Rockstuhl C, Guo G, Guo G, Tame M and Ren X 2018 *Optica* **5** 1229-1235
[6] Moreno E, Garcia-Vidal F J, Erni D, Cirac J I and Martín-Moreno L 2004 *Phys. Rev. Lett.* **92** 236801
[7] Fasel S, Robin F, Moreno E, Erni D, Gisin N and Zbinden H 2005 *Phys. Rev. Lett.* **94** 110501
[8] Ren X-F, Guo G-P, Huang Y-F, Li C-F and Guo G-C 2006 *Europhys. Lett.* **76** 753–9

[9] Schouten H F, Kuzmin N, Dubois G, Visser T D, Gbur G, Alkemade P F A, Blok H, 't Hooft G W, Lenstra D and Eliel E R 2005 *Phys. Rev. Lett.* **94** 053901
[10] Fasel S, Halder M, Gisin N and Zbinden H 2006 *New J. Phys.* **8** 13
[11] Akimov A V, Mukherjee A, Yu C L, Chang D E, Zibrov A S, Hemmer P R, Park H and Lukin M D 2007 *Nature* **450** 402–6
[12] Kolesov R, Grotz B, Balasubramanian G, Stöhr R J, Nicolet A A L, Hemmer P R, Jelezko F and Wrachtrup J 2009 *Nat. Phys.* **5** 470–4
[13] Di Martino G, Sonnefraud Y, Kéna-Cohen S, Tame M, Ozdemir S, Kim M S and Maier S A 2012 *Nano Lett.* **12** 2504–8
[14] Cai Y-J, Li M, Ren X-F, Zou C-L, Xiong X, Lei H-L, Liu B-H, Guo G-P and Guo G-C 2015 *Phys. Rev Applied* **2** 014004
[15] Huck A, Smolka S, Lodahl P, Sørensen A, Boltasseva A, Janousek J and Andersen U L 2009 *Phys. Rev. Lett.* **102** 246802
[16] Gonzalez-Tudela A, Martin-Cano D, Moreno E, Martin-Moreno L, Tejedor C and Garcia-Vidal F J 2011 *Phys. Rev. Lett.* **106** 020501
[17] Heeres R W, Kouwenhoven L P and Zwiller V 2013 *Nat. Nanotech.* **8** 719–22
[18] Dutta Gupta S and Agarwal G S 2014 *Opt. Lett.* **39** 390–3
[19] Fakonas J S, Lee H, Kelaita Y A and Atwater H A 2014 *Nat. Photon.* **8** 317–20
[20] Steel M 2014 *Nat. Photon.* **8** 273–5
[21] Di Martino G, Sonnefraud Y, Tame M S, Kéna-Cohen S, Dieleman F, Özdemir Ş K, Kim M S and Maier S A 2014 *Phys. Rev. Appl.* **1** 3
[22] Gorodetski Y, Bliokh K Y, Stein B, Genet C, Shitrit N, Kleiner V, Hasman E and Ebbesen T W 2012 *Phys. Rev. Lett.* **109** 013901
[23] Jacob Z and Shalaev V M 2011 Plasmonics goes quantum *Science* **334** 463–4
[24] Tame M S, McEnery K R, Özdemir Ş K, Lee J, Maier S A and Kim M S 2013 *Nat. Phys.* **9** 329–40
[25] Nielsen M A and Chuang I L 2010 *Quantum Computation and Quantum Information* (Cambridge: Cambridge university press) (https://doi.org/10.1017/CBO9780511976667)
[26] Aharonovich I, Greentree A D and Prawer S 2011 *Nat. Photon.* **5** 397–405
[27] Huck A, Kumar S, Shakoor A and Andersen U L 2011 *Phys. Rev. Lett.* **106** 096801
[28] Kubo W and Fujikawa S 2011 *Nano Lett.* **11** 8–15
[29] Kwiat P G, Waks E, White A G, Appelbaum I and Eberhard P H 1999 *Phys. Rev.* A **60** R773
[30] Cormann M, Remy M, Kolaric B and Caudano Y 2016 *Phys. Rev.* A **93** 042124
[31] Ungureanu S, Kolaric B, Chen J, Hillenbrand R and Vallée R A L 2013 *Nanophotonics* **2** 173–85
[32] van der Veen M A, Rosolen G, Verbiest T, Vanbel M K, Maes B and Kolaric B 2015 *J. Mater. Chem.* C **3** 1576–81
[33] Altepeter J B, James D F V and Kwiat P G 2004 4 Qubit Quantum State Tomography *Quantum State Estimation* (*Lect. Notes Phys.* 649) ed) ed M Paris and J Řeháček (Berlin, Heidelberg: Springer) 4 113–45
[34] Altepeter J B, Jeffrey E and Kwiat P G 2005 *Advances in Atomic, Molecular and Optical Physics* **52** 105–59
[35] Johnson P B and Christy R W 1972 *Phys. Rev.* B **6** 4370–9
[36] Johnson P B and Christy R W 1974 *Phys. Rev.* B **9** 5056–70
[37] Polyanskiy M Refractive index database https://refractiveindex.info/